ELSEVIER

Journal of Nuclear Materials 241–243 (1997) 517–521

journal of nuclear materials

Calculation of power deposition patterns on the ergodic divertor

Ph. Ghendrih *, A. Grosman

Association Euratom-CEA, DRFC, CEA Cadarache, F-13108 St. Paul-lez-Durance Cédex, France

Abstract

Energy deposition on the vented target plate of the ergodic divertor is analyzed. Shadowing is shown to depend on short parallel excursions. Short excursions also determine the radial penetration of the flux tubes and hence the poloidal phase of the field line with the magnetic perturbation. The latter feature is shown to govern the energy deposition patterns. A WKB calculation allows one to relate the field line radial excursion to the deposited energy flux. The good agreement between the experimental results and the model demonstrates that the calculation yields a comprehensive procedure to simulate power fluxes to all parts of the first wall.

Keywords: Tokamak; Tore Supra; Ergodic divertor; 3D model; Energy deposition

1. Introduction

On Tore Supra, the main areas of energy deposition are actively cooled [1]. On such elements an overshoot in the deposited power will not lead to a self healing process like a carbon bloom but to severe damage of the cooling system [2]. In view of increasing the performance capability of the ergodic divertor [3] it is thus essential to precisely analyze the energy deposition pattern on the ergodic divertor module itself. Owing to the complex geometry of the module they are large areas where the power deposition cannot be measured with the infrared imaging system [4]. It is therefore of the highest importance to compute the energy deposition pattern. The available measurements are used to validate the calculation.

2. Energy transport in a stochastic boundary

The Tore Supra ergodic divertor is based on a resonant magnetic perturbation of the equilibrium magnetic fields [3]. The helical radial magnetic perturbation is generated by six identical coils (toroidal width $\delta\varphi = 14°$ each) equally spaced toroidally. The coils lie on a torus with major radius $R_{ED} = 2.38$ m and minor radius $a_{ED} = 0.8$ m. The toroidal periodicity of the magnetic perturbation is therefore $\Delta\varphi = 60°$ determining the main toroidal wave number $\bar{n} = 6$. The coils have a poloidal extent of $\delta\theta \sim 120°$ which determines the poloidal width of the spectrum, $\delta m \sim 6$. They are located on the low field side of the torus so that the perturbation is negligible on the high field side. The poloidal wave number of the perturbation, $\bar{m} \approx 18$ for $\beta_p + l_i/2 \sim 0.7$, is induced by the poloidal periodicity of the perturbing current flowing in the coil, $I_{ED} \leq 45$ kA. The resonant safety factor of the device, $q_{res}\ (\rho = 1) = \bar{m}/\bar{n}$, is such that a field line experiences 3 to 4 radial steps on the low field side with no radial step on the high field side.

The actively cooled target plates are located between the current bars where the radial component of the magnetic field is the largest. The target plates extend poloidally over 8° and are inclined outwards. The constraint for a point r_0, θ_0, φ_0 located on the target plate is $r_0 = a_{ED} + ((R_{ED} + a_{ED})(\delta\varphi/2 - \varphi_0))\tan(\alpha_{target})$. In the present investigation we consider a flat target plate, hence neglecting the structure along θ_0. The angle between the prototype target plate and the toroidal field is $\alpha_{target} \sim 14°$. It determines the radial penetration of the target plate between the current bars, $\Delta r_{target} \sim 0.065$ m.

The analysis of the energy deposition on the ergodic divertor is two fold, on the one hand there is the balance

* Corresponding author. Tel.: +33-4 4225 2993; fax: +33-4 4225 6233; e-mail: ghendrih@drfc.cad.cea.fr.

PII S0022-3115(96)00556-9

between parallel and transverse heat diffusion ($\chi_{\parallel}$ and $\chi_{\perp}$ respectively), and on the other hand one must account for the stochastic features of the field lines characterized by two scales. On short parallel scales, $L_{\parallel} \leq L_K$, field lines experience the exponential divergence governed by the Kolmogorov length, L_K [3]. On long parallel scales, $L_{\parallel} \gg L_K$, transport is governed by the field line diffusion, D_{FL} ($\sim 10^{-4}$ m^2/m) [3]. In a standard approach where energy diffusion is superimposed to field line stochasticity, one finds an effective radial heat diffusivity given by $\chi_{erg} = D_{FL}\chi_{\parallel}L_T$ [3], where L_T is the coherence length of the temperature field. The latter scale is the Kolmogorov length with a logarithmic contribution due to the transport balance, $L_T = L_K \log(\alpha_T)$ where $\alpha_T^2 = \chi_{\parallel} D_{FL}/(\chi_{\perp} L_K)$. For each point in the divertor volume, the scale L_T separates the connected points into a region governed by the exponential divergence of the field lines, termed the laminar region, and a region governed by the diffusion process beyond the laminar region. The energy deposition capability of a given flux tube in the boundary will therefore reflect both the geometrical features of the flux tubes which characterizes the laminar transport and the effectiveness of the heat transport to such a flux tube which is governed by the diffusion regime.

3. Shadowing of the target plates

Let us now consider a field line impinging onto the prototype vented target plate at $(r_0, \theta_0, \varphi_0)$ [4]. As one follows the field line away from the target plate, the field line will experience two to three radial steps over $3\Delta\varphi$ toroidal turns. In a situation close to the resonance these steps will be inwards and depend on the exact position of the starting point on the neutralizer plate. Let us introduce the radial penetration of the field line $\delta r = r(3\Delta\varphi) - a_{ED}$. The cosine like poloidal dependence of the magnetic perturbation governs the following approximation of δr, $\delta r(r_0, \theta_0, \varphi_0) = \Delta r(\delta b_r, r_0)\cos(m(\theta_0 - \bar{\theta}(r_0)))$. The radial position and the normalized magnetic perturbation $\delta b_r = \delta B_r/B_T$ determine the maximum of δr against θ_0. This approximation is compared to the output from Mastoc (field line tracing code [3]). The magnetic equilibrium considered here is a standard $q = 3$ configuration at low toroidal field, $B_T \approx 2$ T. On Fig. 1, δr is plotted versus θ_0. The clear departure from the poloidal mid value, $\bar{\theta}(a_{ED}) = 4°$, is due to a shear effect which can be estimated to 1.8° ($\bar{\theta}(a_{ED}) \approx 5.8°$) in agreement with the code output. The shear effect and the departure of the radial magnetic perturbation from the cosine dependence leads to a fit with $m = 23$ instead of $\bar{m}$, the mode number of the perturbation. This dependence on θ_0 determines the poloidal shape of the energy deposition patterns discussed in Section 4.

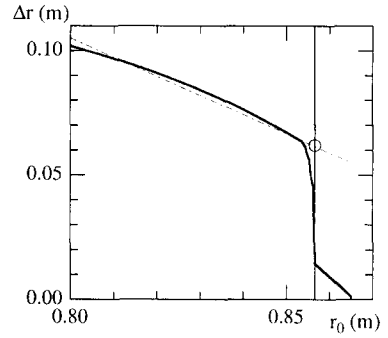

Fig. 2. Dependence of the radial penetration Δr on the radial position on the target plate after $3\Delta\varphi$ toroidal steps. The vertical line at r_{0s} indicates the position of the boundary of the wetted region.

The dependence of Δr on r_0 is illustrated on Fig. 2. For $r_0 \leq r_{0s} \sim 0.86$ m, the relationship is close to linear. Beyond r_{0s}, there is a sudden drop of Δr which is indicative of a shadowing effect. This shadowing is due to the divertor coil itself. It reduces the wetted fraction of the target plate defined by $S_{wetted} = 1 - (r_{0s} - a_{ED})/\Delta r_{target}$.

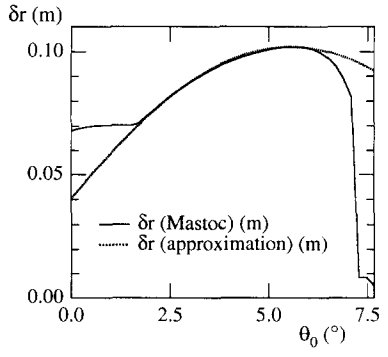

Fig. 1. Radial penetration of the field lines starting at $r_0 = a_{ED}$ versus the poloidal position on the target plate after $3\Delta\varphi$ toroidal steps. The dashed curve is the cosine approximation.

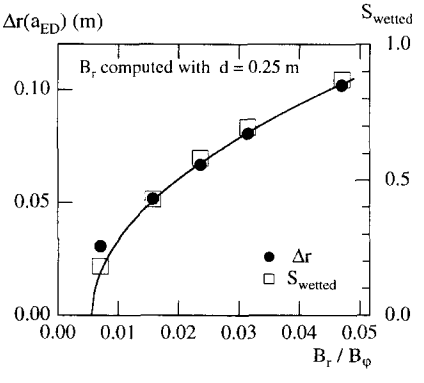

Fig. 3. Dependence of the radial penetration Δr and wetted fraction of the target plate S_{wetted} on the normalized perturbation $\delta B_r/B_\varphi$. (d is the distance between the current bars).

For a series of calculations where the radial perturbation δB_r (determined by I_{ED}) and the toroidal field B_T are varied, Fig. 3, one finds that Δr and the wetted fraction of the target plate, S_{wetted}, exhibit the same dependence on $\delta b_r = \delta B_r / B_T$, namely, the standard square root dependence with a threshold at 5.6×10^{-3} [3]. In order to reach a full wetting of the target plate one would have to increase the perturbation level to $\delta b_r \sim 0.06$ ($B_T \sim 1.6$ T, $I_{ED} = 45$ kA). Such a magnitude of the perturbation is in conflict with the limitation of the perturbation on the $q = 2$ surface stemming from MHD stability issues [5]. This has led to reduce the target plate inclination to $\alpha_{target} \approx 7°$ in the new design of the vented target plates.

4. Energy deposition patterns on the target plates

The short toroidal excursions determine the wetted surface of the target plate but do not yield the observed deposition patterns. The latter are governed by the series of radial steps which occur as the toroidal excursion is further increased. In a first sequence of steps $\Delta\varphi$, the field line moves out of the perturbed region so that the radial position is unchanged and the variation of the poloidal angle is determined by the safety factor $q(r_0 + \Delta r)$, Fig. 4. Let $N\Delta\varphi$ be the toroidal angle such that the field line has returned to the low field side before experiencing a new series of radial steps, $N \sim q\bar{n}$. Depending on the phase of the field line with respect to the perturbation and hence on the poloidal angle $\theta_N = \theta(\varphi = N\Delta\varphi)$, the field line will either experience radial steps outwards, reconnecting the field line to a target plate, or steps inwards, connecting the field line towards the core plasma, Fig. 4. The constraint on the values of θ_N which ensure a connection to the energy source determines the 'hot' patterns on the target plate. Using the dependence of θ_N on the safety factor and therefore on Δr and hence r_0, Fig. 2, one can compute analytically the relation between the number of toroidal steps N performed in the calculation and the number of patterns and their position. A careful comparison between the measured patterns and the computed patterns allows one to determine the matching value of N, $N_T = (q/q_{res})(\bar{m} + 2)$ for typical ohmic shots. This analysis provides an experimental measure of L_T, $L_T = (\bar{n}\Delta\varphi)qR(1 + 2/\bar{m})$.

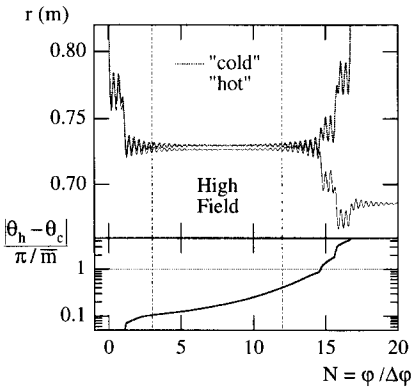

Fig. 4. Field line tracing of a 'cold' and a 'hot' field line. The two field lines start from neighboring positions on the target plate and reach similar radii after 3 steps, upper curve. During the high field side steps, the poloidal distance increases, lower curve, reaching $\pi/\bar{m}$ as the field line returns to the low field side. This corresponds to half the period of the perturbation so that the two field lines exhibit completely different behaviors onwards. The 'hot' field line penetrate further towards the plasma core while the 'cold' field line is deflected back to the divertor.

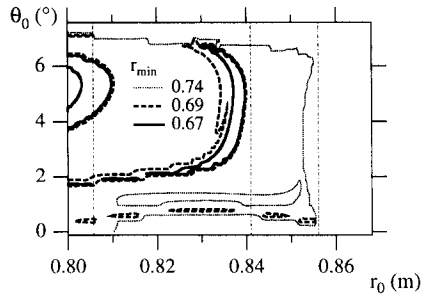

Fig. 5. 2D contour map on the target plate surface of the minimum radius r_{min} experienced by a field line over one poloidal turn (Mastoc criterion). The vertical lines indicate the analytically determined location of the patterns. Low toroidal field calculation, $B_T \sim 2$ T.

Mapping the minimum radius r_{min} reached during $N\Delta\varphi$ toroidal steps starting from the target plate, the Mastoc criterion [3], one recovers these structures, Fig. 5. The analytical calculation of the patterns and their location on the plate for this $\delta b_r = 0.047$ configuration shows that the two main structures correspond to $N = 14$ and $N = 15$. The pattern on the poloidal side bands of Fig. 5 corresponds to the $N = 16$ structure.

5. 'E-folding length' of the energy flux in a stochastic boundary

The relation between the radial excursion of a given field line and the parallel power flux to the target plate is derived from the standard calculation of the SOL e-folding lengths.

$$\chi_\perp \frac{d^2\left(\frac{3}{2}nT\right)}{dr^2} = -\frac{\frac{3}{2}nT}{\tau_\parallel}\,;\ \tau_\parallel = \frac{\left(L_{wall}\exp(L_{wall}/L_T)\right)^2}{\chi_\parallel} \tag{1}$$

The difference with the standard SOL calculation is introduced by the long connection lengths to the wall $L_{wall}(r)$ and there radial dependence. when this connection length is larger than the scale L_T, the probability for a direct

parallel deposition of energy along the given field line decreases. This effect is due to the combined effect of the stochasticity of the field line and of the transverse transport. Owing to the radial dependence of the connection properties one is led to introduce a local e-folding length of the energy $\lambda(r)$.

$$\lambda(r) = \sqrt{\frac{\chi_\perp}{\chi_\parallel}}\, L_{\mathrm{wall}} \exp(L_{\mathrm{wall}}/L_{\mathrm{T}}) \qquad (2)$$

Following the WKB procedure in the domain where the scale of variation of $\lambda(r)$ is much larger than $\lambda(r)$ itself, one obtains the radial dependence of the parallel heat flux for a stochastic field line exhibiting a radial penetration from a_{ED} to r.

$$Q_\parallel(r_0, \theta_0) \propto \sqrt{\chi_\parallel \chi_\perp} \exp\left(-\int^r \frac{\mathrm{d}r}{\lambda(r)}\right) \Big/ \sqrt{\lambda(r)} \qquad (3)$$

The connection length to the wall is determined by $\Sigma(\Delta r)^2/D_{\mathrm{FL}}$. Adding the contributions from the various resonances leads to:

$$L_{\mathrm{wall}}(r) = \int_r^{a_{\mathrm{ED}}} \mathrm{d}r \frac{\Delta_{\mathrm{res}}(r)}{D_{\mathrm{FL}}(r) H(\sigma_{\mathrm{Chir}}(r) - \sigma^*_{\mathrm{Chir}})} \qquad (4)$$

Δ_{res} is the distance between neighboring resonances. The Heaviside function H governs the threshold of the stochastic diffusion in terms of the Chirikov parameter [3], $\sigma_{\mathrm{Chir}} \geq \sigma^*_{\mathrm{Chir}} \sim 1$.

The relationship between the deposited energy flux and the radial excursion of a field line, as computed from Eqs. (1)–(3), is depicted on Fig. 6. The output of the calculation is the curve labelled $Q_\parallel$. Starting from the wall and increasing the radial excursion of the field line, hence increasing the connection length to the wall, one finds three regimes. In the vicinity of the wall the available energy flux is vanishingly small, i.e. the field lines with short connection lengths do not contribute to the energy exhaust. In a second region, the energy extraction capability rapidly increases. However, as the connection length further increases this extraction capability levels off and finally decreases in the third regime. In the later regime, the connection length is long enough to allow for the transverse energy transport to neighboring flux tubes. For the very long connection lengths, a balance between the transverse outflux and influx is to be introduced so that there is no effective roll over to the third regime. Beyond the stochastic boundary, the increase of the energy flux is governed by the decrease of the area of the flux surfaces. Radiation or charge exchange losses have not been incorporated in the transport process although they can induce significant changes in the energy removal channels [6,7]. Changing the transport balance by increasing the ratio $\chi_\perp/\chi_\parallel$ will lower the peaking factor of the energy deposition by feeding flux lines with short connection lengths, Fig. 6.

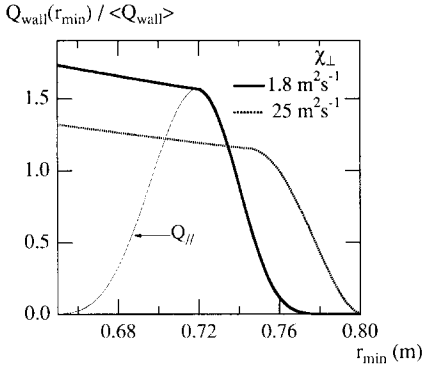

Fig. 6. Normalized parallel heat flux impinging onto the surface of the target plate versus the minimum radial penetration experienced by the flux tube over one poloidal turn. Increasing the transverse transport or lowering the parallel transport will feed the field lines with a smaller penetration and thus reduce the peaking factor, dashed curve.

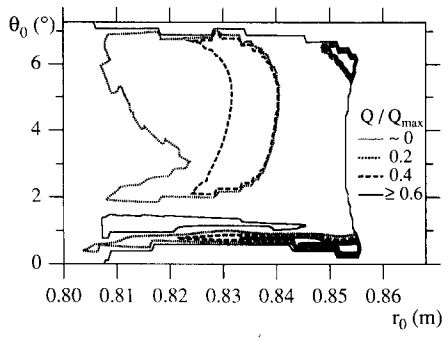

Fig. 7. Computed 2D energy flux contours on the 'flat' target plate. The contour lines are normalized by the maximum of the energy flux. Low toroidal field calculation, $B_{\mathrm{T}} \sim 2$ T.

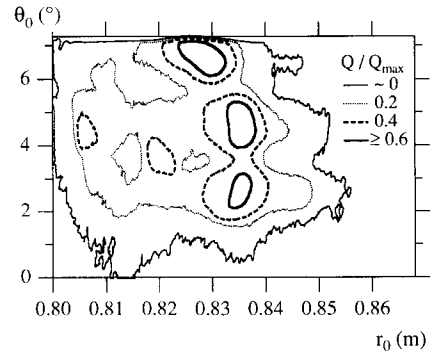

Fig. 8. Experimental 2D energy flux contour on the vented target plate. As on Fig. 7, the contour lines are normalized by the maximum of the measured energy flux. Data of this figure is obtained from an infrared image of the prototype target plate in a low toroidal field experiment, $B_{\mathrm{T}} \sim 2$ T.

Using the computed relation between the radial excursion and the normalized energy flux, Fig. 6, one can map the r_{min} contour plot, Fig. 5, into a parallel energy flux impinging onto the target plate. With the knowledge of the inclination of the field lines with respect to the target plate, one can compute the actual energy flux to the target plate. The energy flux impinging onto the 'flat' target plate is characterized by two patterns, Fig. 7. One of these patterns is made of the side bands of the shadowed $N = 16$ pattern. This relative increase in magnitude is due to the larger radial magnetic field at the boundary of the target plate. The second structure, the $N = 15$ pattern is located at mid target while the $N = 14$ structure located on the left hand side of Fig. 5 is smeared out due to a compensation between the divertor and ripple radial component Fig. 7. Owing to the viewing angle of the vented target plate by the infrared camera, the lower third of the target plate is gradually shadowed as its surface is lowered behind the front face, Fig. 8. This effect does not allow one to image the peaked $N = 16$ structure located on the lower part of the target plate. Furthermore, the image does not include the top right the region where the calculation predicts another part of the peaked $N = 16$ deposition pattern. As in the calculated deposition pattern, the clearest structure is the mid-target structure. One finds a similar peaking factor, and the same location on the target plate.

6. Conclusion

The energy deposition on the target plate of the ergodic divertor has been fully analyzed. The shadowing of the target plate has been shown to be a short scale effect governed by the ripple and the ratio of the radial magnetic perturbation to the main toroidal field δb_r. Both the wetted surface and the maximum radial penetration of the field lines on very short scales follow a standard square root dependence on δb_r. The observed patterns are shown to be governed by the poloidal phase of the flux tubes with respect to the magnetic perturbation. The poloidal phase of the field lines is governed by the shear along the unperturbed trajectory on the high field side, and therefore by the radial penetration on the short scale. This relationship allows one to determine analytically the location of the patterns.

In order to complete the analysis, a WKB approximation of the energy transport in the laminar region yields the deposited parallel energy flux in terms of the radial penetration of a field line over the typical parallel coherence scale. Using the computed angle between the field line and the target plate one can check the calculation with the experimental deposited energy flux. Agreement on both the peaking and position of the patterns is obtained. This gives us confidence that present calculations will allow to determine the energy deposition on poorly imaged parts of the ergodic divertor coils.

References

[1] P. Chappuis et al., presented at 12th Int. Conf. on Plasma Surface Interactions, May 1996, Saint-Raphaël, France.
[2] R. Nygren et al., these Proceedings, p. 522.
[3] Ph. Ghendrih, A. Grosman and H. Capes, Plasma Phys. Control. Fusion 38 (1996) 1653.
[4] A. Grosman et al., these Proceedings, p. 532.
[5] S. Turlur et al., these Proceedings, p. 548.
[6] H. Capes et al., Phys. Fluids B 4 (1992) 1287.
[7] Ph. Ghendrih et al., J. Nucl. Mater. 220–222 (1995) 305.